PHOTONICS Research

First demonstration of an on-chip quadplexer for passive optical network systems

Dajian Liu,[1] Long Zhang,[1] Hexin Jiang,[1] and Daoxin Dai[1,2,*]

[1]State Key Laboratory for Modern Optical Instrumentation, Center for Optical & Electromagnetic Research, College of Optical Science and Engineering, International Research Center for Advanced Photonics, Zhejiang University, Hangzhou 310058, China
[2]Ningbo Research Institute, Zhejiang University, Ningbo 315100, China
*Corresponding author: dxdai@zju.edu.cn

Received 22 January 2021; revised 1 March 2021; accepted 1 March 2021; posted 1 March 2021 (Doc. ID 420545); published 26 April 2021

An on-chip quadplexer is proposed and demonstrated with four wavelength-channels of 1270, 1310, 1490, and 1577 nm. The present quadplexer consists of four cascaded filters based on multimode waveguide grating (MWG), which are composed of a two-mode (de)multiplexer and an MWG. For the fabricated quadplexer on silicon, all four wavelength channels have flat-top responses with low excess losses of <0.5 dB as well as the desired bandwidths, which are about 16, 38, 19, and 6 nm, respectively. The cross-talk for both upstream channels and downstream channels is less than −24 dB. Moreover, the data transmission of 10 Gb/s of the present silicon quadplexer is also successfully demonstrated.

https://doi.org/10.1364/PRJ.420545

1. INTRODUCTION

Driven by the rapid development and popularization of high-traffic and high-bandwidth services such as 4 K/8 K video and virtual reality, passive optical network (PON) architectures have been quickly evolving [1–4], providing enhanced availability, data rates, and services. The original GPON (gigabit PON) cannot satisfy some users' requirements anymore, and it is a general trend to upgrade the GPON to be 10G GPON. On the other hand, not every user needs to immediately upgrade their service; GPON and 10G GPON usually coexist in an optical distribution network, which will last for a long time. As a point-to-multipoint network architecture, a PON consists of several optical network units (ONUs) near end users and an optical line terminal (OLT) at the service provider's central office. According to the ITU-T G.987.4 standard, the upstream and downstream center wavelengths of GPON and 10G GPON are 1310/1490 nm and 1270/1577 nm, respectively, as shown in Fig. 1(a). For a smooth transition from GPON to 10G GPON, a quadplexer should be introduced as a special wavelength division multiplexer (WDM) to combine/separate the wavelength channels of GPON and 10G GPON signals, to satisfy the coexistence requirements of the GPON and the 10G GPON, as shown in Figs. 1(b) and 1(c). The quadplexers used in the systems were developed with some discrete components, which are cumbersome. More importantly, it prevents the monolithic integration with other components (such as optical modulators and photodetectors) to realize on-chip transceivers, which is necessary for next-generation PON systems operating with very high bit rates. Therefore, it is important to develop high-performance on-chip quadplexers with compact footprints.

As it is well known, silicon photonics has become very promising because of CMOS compatibility, low waveguide loss, and high integration density. Numerous silicon photonic devices have been demonstrated successfully for data transmission [5–9]. In particular, for PON systems, lots of special photonic components are needed [10–12], such as diplexers, triplexers [13–15], and quadplexers [16]. Among them, diplexers and triplexers have been developed successfully with silicon photonic technology in recent years. In contrast, it is still a big challenge to develop on-chip quadplexers due to the special requirements for the wavelengths as well as the bandwidths of the four channels. To the best of our knowledge, no on-chip quadplexer has been reported yet.

As shown in Figs. 1(a)–1(c), a quadplexer is proposed to realize the co-existence of GPON and 10G GPON by combining the two channels of 1270/1310 nm for downloading and the two channels of 1490/1577 nm for uploading. The corresponding bandwidths for these four channels are 20, 40, 20, and 5 nm, respectively. There have been several typical on-chip WDMs using for example, arrayed-waveguide gratings (AWGs) [17,18], etched diffraction gratings (EDGs) [19], microring resonators (MRRs) [20], and Mach–Zehnder interferometers (MZIs) [21,22]. According to the working principle, AWGs and EDGs are suitable for multichannel WDM systems with uniform channel spacing in a wavelength range limited by the free spectral range (FSR). Even though a novel cross-order silica AWG triplexer with three channels of 1310/1490/1550 nm was proposed to break the FSR limitation [18], it is still

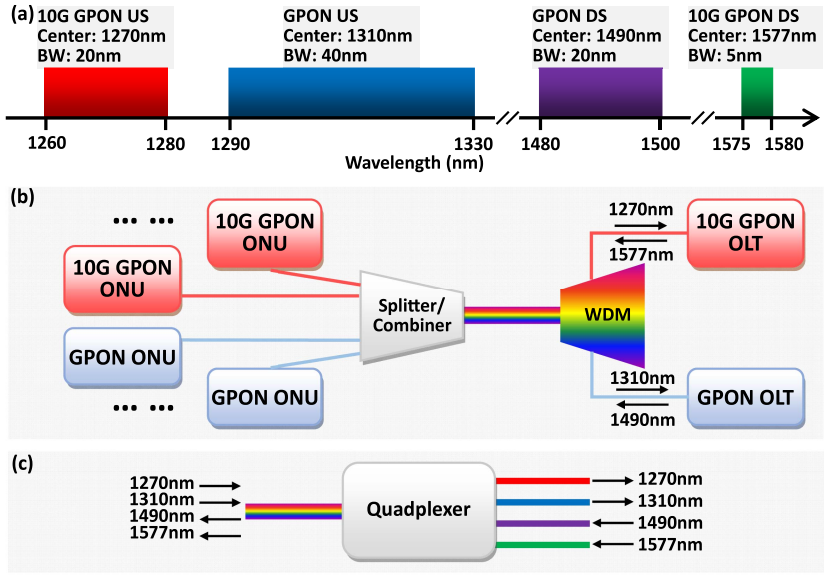

Fig. 1. (a) PON wavelength plan. US, upstream; DS, downstream; BW, bandwidth. (b) PON configuration with the coexistence of GPON and 10G GPON. (c) Structure schematic diagram of a quadplexer.

inflexible for AWGs/EDGs to achieve nonuniform bandwidths as desired for triplexers as well as the quadplexers considered in this paper. Similarly, WDMs based on cascaded MZIs do not have nonuniform channel spacing as desired and the wavelength range is also limited by the FSR. Furthermore, it usually requires critical control of the phase shifts and the coupling ratios for MZIs, which causes fabrication challenges. When using MRRs, designers can make the channel wavelengths flexible and the channel bandwidth is also flexible. However, the bandwidth is usually 1–2 nm or less and the FSR is only several tens of nanometers, according to the minimum bending radius. As a result, MRR-based WDMs also do not provide a channel bandwidth as wide as 5–40 nm and an operation wavelength range as wide as ~300 nm. In summary, it is difficult to realize such a quadplexer with highly nonuniform broad bandwidths (i.e., 5–40 nm) and very sparse channels in a 300 nm wide wavelength range from 1270 nm to 1577 nm by using regular photonic filters, such as AWGs/EDGs, MRRs, and MZIs.

In this paper, we propose and demonstrate what we believe, to the best of our knowledge, is the first on-chip quadplexer by using four cascaded multimode waveguide grating (MWG) filters. Previously, we realized a four-channel coarse wavelength division (de)multiplexer based on cascaded MWGs that works well in the 80 nm wide O-band covering the channels of 1271/1291/1311/1331 nm to satisfy the demands in short-distance optical interconnects (e.g., data centers) [23]. Recently, a silicon-based on-chip triplexer was also realized with three cascaded MWGs for the three channels of 1310/1490/1550 nm in fiber-to-the-home (FTTH) systems [24]. For the realized triplexer, the challenge is to design the MWGs carefully with optimized apodization strengths, corrugation depths, and periods, to achieve low losses and low cross-talk as well as the desired bandwidths of 100, 20, and 10 nm for the channels of 1310, 1490, and 1550 nm, respectively. In contrast, the design for the MWGs for the present on-chip quadplexer is even more challenging because of the ultrawide operation wavelength range covering the O-, S- and L-bands (i.e., 1270/1310/1490/1577 nm) and their nonuniform bandwidths of 20/40/20/5 nm. It means that one should carefully take the waveguide dispersion and the grating effects for more than one mode into account. Fortunately, four MWG-based filters were successfully designed with satisfactory performances. For the fabricated on-chip quadplexer, flat-top responses have been achieved with low excess losses of <0.5 dB and low cross-talk of < -24 dB for all channels. Such a compact silicon-based, on-chip quadplexer with excellent performances can be easily integrated with other silicon photonic devices and thus will be useful for PON systems.

2. STRUCTURE AND DESIGN

Figure 2(a) shows the proposed quadplexer on silicon, which consists of four cascaded MWG-based filters with flat-top responses. Each MWG-based filter is composed of an apodized MWG and a TE_0/TE_1 mode (de)multiplexer based on an adiabatic taper, as shown in Fig. 2(b). Here, the MWGs are used to convert the launched TE_0 mode to the reflected TE_1 mode for the wavelength-band around the Bragg wavelength. Then the backward TE_1 mode is converted to the TE_0 mode through the mode (de)multiplexer and outputs at the drop port in the end, as shown in Fig. 2(b). For these four MWG-based filters, the MWGs were designed with Bragg wavelengths of 1270 nm, 1310 nm, 1490 nm, and 1577 nm, respectively.

For the first MWG-based filter operating with the channel of 1270 nm, the TE_0 mode carrying the data is received at the input port, propagates forward, and is then converted to the backward TE_1 mode through the MWG. Finally, it is coupled to the TE_0 mode at output port O_1 through a TE_0/TE_1 mode (de)multiplexer. For the 1310 nm channel, the data carried by the TE_0 mode are also launched at the input port and go

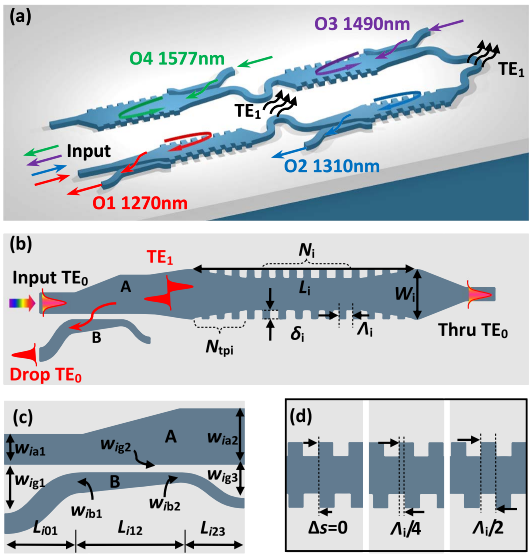

Fig. 2. Schematic configurations: (a) proposed quadplexer; (b) MWG-based filter, consisting of a mode (de)multiplexer and an MWG-based filter; (c) mode (de)multiplexer based on an adiabatic dual-core taper; and (d) longitudinal apodization for the MWG.

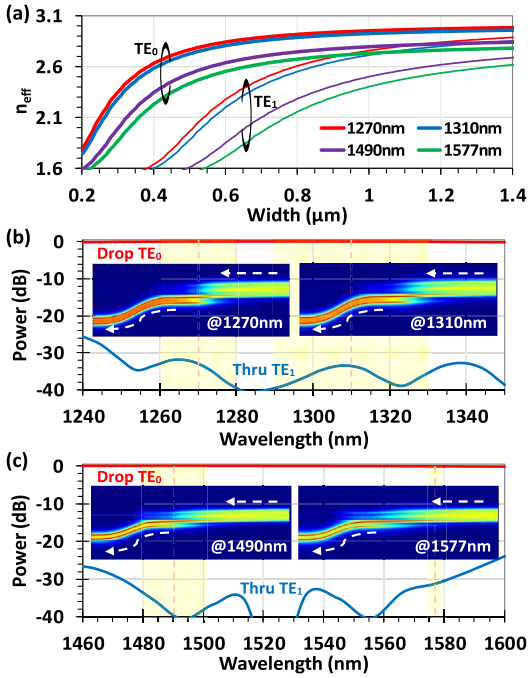

Fig. 3. (a) Calculated dispersion curves of an SOI strip waveguide for the TE_0 and TE_1 modes at four wavelength bands (i.e., 1270, 1310, 1490, and 1577 nm). Simulated transmissions of the designed mode (de)multiplexer for the wavelength band of (b) 1270/1310 nm and the wavelength band of (c) 1490/1577 nm. Insets: simulated light propagation in the designed adiabatic taper.

through the first MWG-based filter with low excess loss and low cross-talk. Similarly, the data for the 1310 nm channel finally drop at port O_2 by the second MWG-based filter. For the 1490 nm and 1577 nm channels, data are launched from ports O_3 and O_4, respectively. For the 1490 nm channel, the launched TE_0 mode from port O_3 is first converted to the TE_1 mode through the TE_0/TE_1 mode (de)multiplexer and then is converted to the reflected TE_0 mode through the third MWG filter. This 1490 nm TE_0 mode goes through the second and first MWG filters successively with low excess loss and low cross-talk and finally exits from the input port. Similarly, the launched data of 1577 nm from port O_4 are manipulated by the fourth MWG-based filter and also finally exit at the input port. In particular, bent waveguides are introduced between any two filters to radiate the residual higher-order mode (TE_1) and greatly reduce the undesired Fabry–Perot resonance.

In the present design, silicon-on-insulator (SOI) strip waveguides with a 220 nm-thick top-silicon layer and a 2 μm thick oxide buffer are chosen. A 1.2 μm thick SU-8 upper cladding was chosen for fabrication convenience. One can also choose cladding materials such as SiO_2. Figure 3(a) shows the dispersion curves for the TE_0 and TE_1 modes in the 220 nm thick SOI waveguide when operating at wavelengths of 1270, 1310, 1490, and 1577 nm, respectively. Here, the mode (de)multiplexers based on dual-core adiabatic couplers were used, as shown in Fig. 2(c). They are designed according to the calculated dispersion curves in Fig. 3(a), following the method proposed in our previous work [25]. Here, some careful optimization is made for the design of the quadplexer with specific channel wavelengths and channel bandwidths.

Regarding the ultrawide working wavelength range for the quadplexer, two broadband TE_0/TE_1 mode (de)multiplexers are designed, respectively, for the wavelength channels of 1270/1310 nm and 1490/1577 nm. For the wavelength channels of 1270/1310 nm (i.e., $i = 1, 2$), the core widths at the input/output ends of waveguides A and B for the adiabatic coupler are chosen as $(w_{ia1}, w_{ia2}) = (450, 550)$ nm, and $(w_{ib1}, w_{ib2}) = (250, 120)$ nm, respectively. We chose the gap widths $(w_{ig1}, w_{ig2}, w_{ig3}) = (1.2, 0.18, 0.5)$ μm and the taper lengths $(L_{i01}, L_{i12}, L_{i23}) = (25, 35, 5)$ μm. Figure 3(b) shows the calculated wavelength dependence of the transmissions from the TE_1 mode in waveguide A and to the TE_0 mode in waveguide B. From this figure, it can be seen that the designed TE_0/TE_1 mode (de)multiplexer has a low excess loss (<0.05 dB) and a low cross-talk of <-32 dB in the desired wavelength bands around 1270 nm and 1310 nm. For the mode (de)multiplexers for the wavelength channels of 1490 nm and 1577 nm, the parameters are chosen as follows: $(w_{ia1}, w_{ia2}) = (480, 720)$ nm, $(w_{ib1}, w_{ib2}) = (260, 120)$ nm, $(w_{ig1}, w_{ig2}, w_{ig3}) = (1.2, 0.18, 0.5)$ μm, and $(L_{i01}, L_{i12}, L_{i23}) = (20, 35, 5)$ μm. The calculated transmission of the designed TE_0/TE_1 mode (de)multiplexer is shown in Fig. 3(c). It shows that the low excess loss is <0.1 dB and the cross-talk is <-30 dB for the mode (de)multiplexer in the desired wavelength bands around 1490 nm and 1577 nm. The simulated light propagation in the designed mode (de)multiplexers is also shown in the insets when operating at the wavelengths of 1270, 1310, 1490, and 1577 nm, respectively, which verifies the waveguide structure design.

The grating structures are designed according to the phase-matching condition between the TE_0 and TE_1 modes so that the launched TE_0 mode at the input port can be converted to

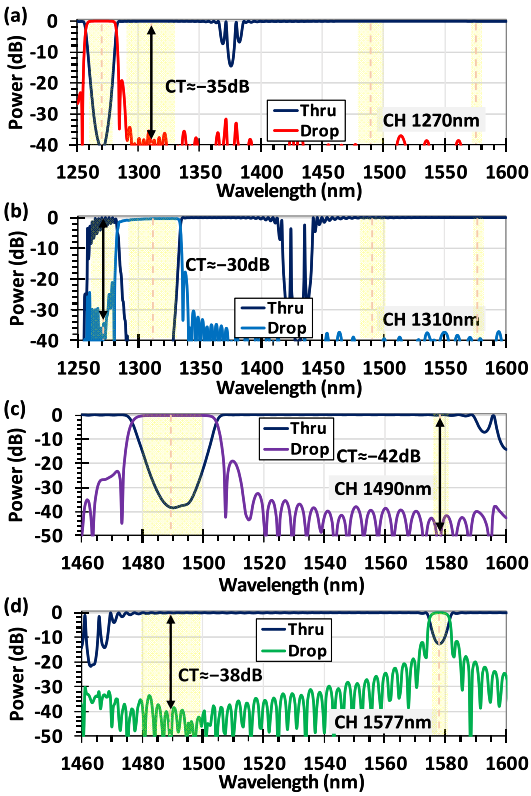

Fig. 4. Calculated transmittance spectra at the drop and through ports for the designed MWGs at the channels of (a) 1270, (b) 1310, (c) 1490, and (d) 1577 nm.

the reflected TE_1 mode. Here, the phase-matching condition is given as $n_{\text{eff}1} + n_{\text{eff}2} = \lambda_B/\Lambda$, where $n_{\text{eff}0}$ and $n_{\text{eff}1}$ are, respectively, the effective indices of the TE_0 and TE_1 modes in the MWG, Λ is the grating period, and λ_B is the Bragg wavelength. Here, grating tapers are introduced to connect the grating section and the input/output section, as shown in Fig. 2(b), to suppress the undesired reflection loss at the front/back ends of the grating section. To improve the sidelobe suppression ratios (SLSRs) and reduce the cross-talk, the grating is apodized longitudinally. For example, the superposition of the gratings is modulated with a Gaussian function of the position z in the propagation direction, as shown in Fig. 2(d) [i.e., $\Delta s = \exp[-b(z - L/2)/L^2]L/2]$, where Δs is the longitudinal shift, b is the apodization strength, and L is the length of the Bragg grating.

From the coupled-mode theory, it is well known that the bandwidth and rejection for the i-th MWG are related to the grating geometry, including the grating width (W_i), the corrugation depth (δ_i), and the grating length (L_i). For the MWGs working for the downloading channels of 1270 nm and 1310 nm, which are close relatives, the gratings are strongly apodized. Figures 4(a) and 4(b) show the calculated spectral responses of the first and second MWGs for the channels of 1270 nm and 1310 nm, respectively. Here, the grating parameters for the first and second MWGs are chosen as follows: the grating widths are $W_1 = W_2 = 850$ nm; the apodization strength is $b_1 = b_2 = 15$; the corrugation depths are $(\delta_1, \delta_2) = (185, 220)$ nm; the grating periods are $(\Lambda_1, \Lambda_2) = (256, 278)$ nm; the numbers of gratings are $(N_1, N_2) = (200, 100)$; and the number of the gratings in taper sections is $N_{1\text{tp}} = N_{2\text{tp}} = 20$. From Figs. 4(a) and 4(b), it can be seen that these two MWGs have bandwidths of 20 nm and 40 nm, respectively, which satisfy the requirements of a quadplexer very well. Both have box-like responses with low excess losses of less than 0.05 dB. The cross-talk between these two channels is less than −30−−35 dB. As shown in Figs. 4(a) and 4(b), the transmissions at the through ports of the first and second MWG-based filters show some drops in the wavelength bands of 1360–1390 nm and 1410–1450 nm. These drops are due to the Bragg grating effects of the forward/backward TE_0 modes. Fortunately, they do not influence the data transmission for the other channels. Here, data carried by the two uploading channels of 1490 nm and 1577 nm can go through these two designed MWGs with very low excess loss. One should notice that for the MWG for the 1310 nm channel, obvious ripples around 1270 nm are observed, which would lead to some notable loss for the 1270 nm channel. Fortunately, this problem can be solved by placing the MWGs for the 1270 nm channel in front of the MWGs for the 1310 nm channel. In this way, the 1270 nm channel is dropped with a low excess loss by the first MWG and thus the second MWG does not introduce any influence on the 1270 nm channel.

Figures 4(c) and 4(d) show the calculated spectral responses for the designed MWG-based filters for the channels of 1490 nm and 1577 nm, respectively. Their parameters are chosen as follows: $W_3 = W_4 = 1100$ nm, $(b_3, b_4) = (15, 5)$, $(\delta_3, \delta_4) = (240, 160)$ nm, $(\Lambda_3, \Lambda_4) = (306, 320)$ nm, $(N_3, N_4) = (200, 300)$, and $N_{3\text{tp}} = N_{4\text{tp}} = 20$. Here, the apodization strengths and the corrugation depths for these two MWGs are chosen quite differently because these two channels are very separate and the bandwidths are very different. In particular, weak apodization strength is chosen for the 1577 nm MWG to achieve a narrow bandwidth of 5 nm. From Figs. 4(c) and 4(d), the designed MWGs have 1 dB bandwidths of 20 nm and 5 nm as desired, respectively. Both have box-like responses with low excess losses of <0.05 dB. When the quadplexer is used as a (de)multiplexer in ONUs, the crosstalk between these two wavelength-channels is −42−−38 dB.

The fabrication tolerance of the designed MWG-based filters is also analyzed by assuming the core width has some deviation of $\Delta w = \pm 10$ nm and ± 20 nm, as shown in Fig. 5, where the MWG for the channel of 1577 nm is analyzed as an example because it has the narrowest bandwidth in the

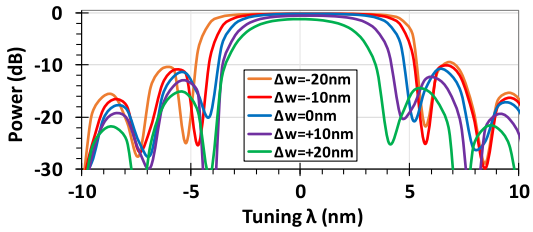

Fig. 5. Simulated transmissions at the drop port of the designed MWG filter at the 1577 nm channel when assuming that there is some core-width variation (i.e., $\Delta w = \pm 10$ nm and ± 20 nm).

quadplexer. Here, the central wavelength shift is not considered. From this figure, it can be seen that the bandwidth of the MWG becomes narrower when the core width is widened. The 1-dB bandwidth $BW_{1\,dB}$ has some deviation of about ± 1.2 nm when $\Delta w = \pm 10$ nm, while the 1-dB bandwidth deviations are $+3$ nm and -1.7 nm when $\Delta w = -20$ and $+20$ nm, respectively. It is shown that the fabrication tolerance for the present quadplexer is similar to many silicon photonic devices and can be acceptable for modern nanofabrication technologies.

3. FABRICATION AND MEASUREMENT

The designed silicon quadplexer was then fabricated on an SOI wafer with a 220 nm thick top-silicon layer and a 2 μm thick buried dioxide layer. The processes of electron beam lithography (150 II, Raith GmbH, Dortmund, Germany) and ICP (inductively coupled plasma) dry-etching were applied to etch through the silicon core. A 1.2 μm SU-8 polymer was spin-coated on the top to be the upper cladding. The microscope and scanning electron microscope (SEM) images of the fabricated quadplexer are shown in Figs. 6(a)–6(g). To characterize the fabricated device operating with an ultrawide wavelength band of >300 nm, several quadplexers with identical structure parameters were fabricated with grating couplers working for the two wavelength bands around 1300 nm and 1530 nm, respectively. The straight waveguides with the same grating couplers are used as the reference for normalization. A super-continuum source (SuperK COMPACT, NKT Photonics A/S, Birkerød, Denmark) and an optical spectrum analyzer (AQ6370D, Yokogawa Electric Corp., Tokyo, Japan) were used to characterize the fabricated quadplexers.

Figures 7(a)–7(d) show the normalized transmittance spectra, which were normalized with respect to the measured transmissions of the straight waveguides with two types of grating couplers. It shows that the measurement results for the four channels agree well with the simulation results. All the four channels have box-like spectral responses with low excess losses

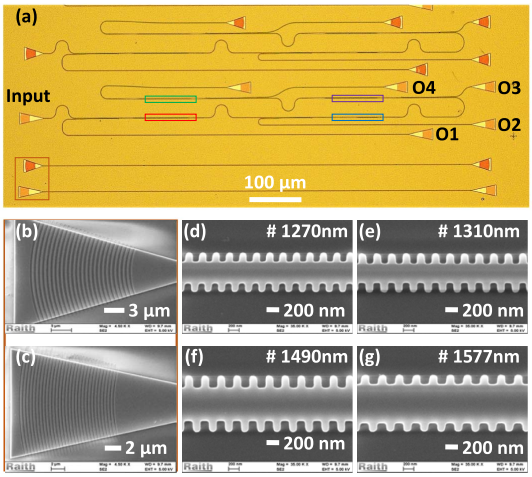

Fig. 6. (a) Microscope image of the fabricated quadplexers on silicon. SEM images of the grating couplers working around (b) 1300 nm and (c) 1530 nm, parts of gratings for (d) 1270 nm, (e) 1310 nm, (f) 1490 nm, and (g) 1577 nm.

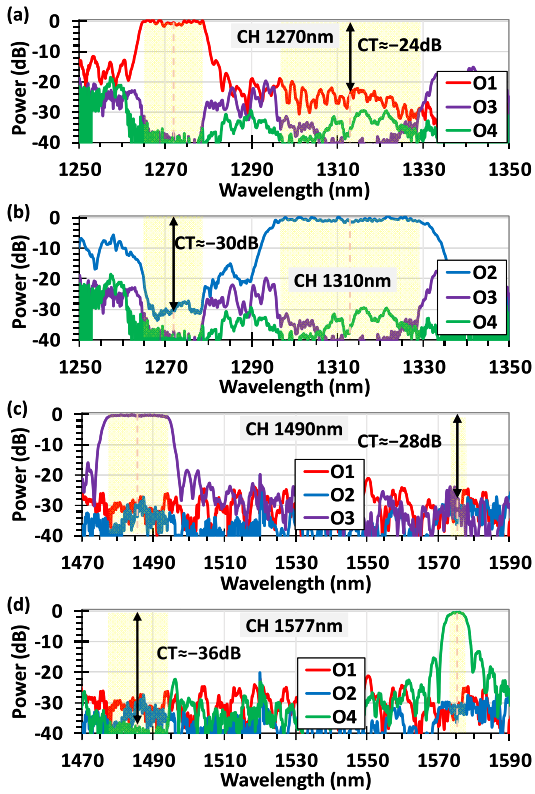

Fig. 7. Measured spectral responses for the four channels of (a) 1270 nm, (b) 1310 nm, (c) 1490 nm, and (d) 1577 nm.

of ~0.5, 0.5, 0.2, and 0.4 dB at the center wavelength, respectively. The bandwidths for the channels of 1270, 1310, 1490, and 1577 nm are 16, 38, 19, and 6 nm, respectively, which are slightly less than the simulated ones due to some fabrication errors. The measured crosstalks for the channels are as low as −30–−20 dB, −32–−28 dB, ~−28 dB, and ~−36 dB, respectively. The performance can be improved further by optimizing the fabrication processes and using the design with cascaded MWGs for each channel. The temperature dependence of all the four channels is also measured experimentally and the measured thermal sensitivities are 51, 45, 56, and 57 pm/°C for channels 1270, 1310, 1490, and 1577 nm, respectively.

The data transmissions with the fabricated quadplexer chip were also carried out by using the setup shown in Fig. 8(a). For the downstream signal (1270 and 1310 nm channels), there were two wavelengths used in the experiment [i.e., $(\lambda_1, \lambda_2) = (1271, 1311)$ nm]. The pulse pattern generators (PPGs) provide non-return-to-zero (NRZ) pseudo random binary sequence signals to the $LiNbO_3$ Mach–Zehnder modulators (MZMs) to generate 10 Gb/s modulated optical signals (according to the ITU-T G.987.4 standard). The two channels of modulated data pass through polarization controllers and are combined using an off-chip CWDM4 multiplexer (MUX). Finally, the data are coupled into the quadplexer chip from the input port and the data carried by the 1271 nm and 1311 nm channels are received from the grating couplers at output ports O_1 and O_2, respectively. For the upstream signals,

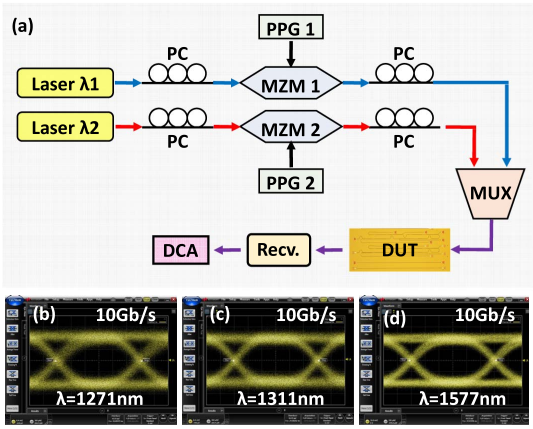

Fig. 8. (a) Measurement setup for the eye diagram, including tunable lasers, polarization controllers (PCs), Mach–Zehnder modulators (MZMs), pulse pattern generators (PPGs), an off-chip multiplexer (MUX), the device under test (DUT), an optical receiver (Recv.), and a digital communication analyzer (DCA). Measured eye diagrams for the channels of (b) 1271 nm, (c) 1311 nm, and (d) 1577 nm.

the 1577 nm channel is considered in the experiment because there are no 1490 nm lasers available in the lab. Figures 8(b)–8(d) show the measured eye diagrams for the data collected from ports O_1, O_2, and O_4, respectively. It shows that the eye diagrams are open with high qualities.

To characterize the nonuniformity of the fabrication for the MWG-based filters in chip-scale, we fabricated an array of identical MWGs on the same chip, as shown in Fig. 9(a). Figure 9(b) shows the normalized measurement results for six samples. It shows that they have very similar spectral responses with similar central wavelengths around ~1593 nm as well as 3 dB bandwidths of ~8.4 nm. Figures 9(c) and 9(d) show the statistical results for the central wavelength (λ) and the 3 dB bandwidth (BW) of the measured samples, respectively. It can be seen that the mean deviations of the central wavelength and the bandwidth are ~0.41 nm and ~0.25 nm, respectively. It shows that the uniformity of the present MWG-based filters is sufficiently excellent for the PON applications and the uniformity can be improved further by using advanced fabrication processes when needed.

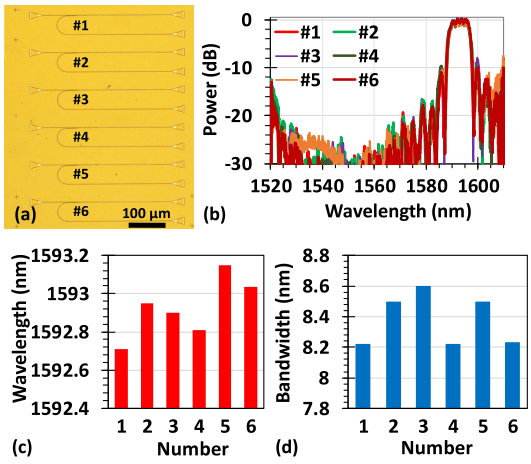

Fig. 9. (a) Microscopy picture of the fabricated identical MWG-based filters; (b) measurement responses at the drop-port; (c) the central wavelength deviation and (d) the 3 dB bandwidth deviation among six samples.

4. SUMMARY AND DISCUSSION

In conclusion, in this paper we have proposed and realized a silicon-based, on-chip quadplexer for the first time, to the best of our knowledge. The quadplexer is designed with four cascaded MWG-based filters. In the present design, apodization gratings, grating tapers, and bent waveguides have been introduced to greatly reduce the cross-talk. All channels for the designed quadplexer have box-like responses with low excess losses (~0.1 dB) and low crosstalk (< −30 dB) in theory. For the fabricated silicon quadplexer, the bandwidths for the wavelength-channels of 1270, 1310, 1490, and 1577 nm are about 16, 38, 19, and 6 nm, respectively. The cross-talk is as low as −30–−20 dB, −32–−28 dB, ~−28 dB, and ~−36 dB for these four channels, respectively. One should notice that the present quadplexer only works for TE polarization. A polarization-insensitive quadplexer can be achieved by introducing an on-chip polarization splitter rotator [26]. In particular, in the present proof-of-concept demonstration, we used two types of grating couplers in the characterization for convenience. On the other hand, edge couplers can be easily used for light coupling between a fiber and a silicon strip waveguide to achieve broadband and polarization-independent coupling. More importantly, the present on-chip quadplexer will be very useful to further develop monolithically integrated transceivers on silicon, which has great potential in reducing the module size and power consumption as well as the package complexity and cost. Furthermore, it is also possible to combine the video signals (1550–1560 nm) and/or optical time-domain reflectometer signals (1625–1675 nm) by cascading two more MWG filters designed with the corresponding central wavelengths and bandwidths. Such a scalable quadplexer with high performances could be used widely to develop next-generation PON and WDM systems.

Funding. National Major Research and Development Program (2018YFB2200200, 2018YFB2200201); National Science Fund for Distinguished Young Scholars (61725503); National Natural Science Foundation of China (61961146003, 91950205); Natural Science Foundation of Zhejiang Province (LD19F050001, LZ18F050001); Fundamental Research Funds for the Central Universities.

Disclosures. The authors declare no conflicts of interest.

REFERENCES

1. V. Houtsma, D. van Veen, and E. Harstead, "Recent progress on standardization of next-generation 25, 50, and 100G EPON," J. Lightwave Technol. **35**, 1228–1234 (2017).
2. J. S. Wey, "The outlook for PON standardization: a tutorial," J. Lightwave Technol. **38**, 31–42 (2020).
3. D. Z. Zhang, D. K. Liu, X. M. Wu, and D. Nesset, "Progress of ITU-T higher speed passive optical network (50G-PON) standardization," J. Opt. Commun. Netw. **12**, D99–D108 (2020).

4. T. Horvath, P. Munster, V. Oujezsky, and N. H. Bao, "Passive optical networks progress: a tutorial," Electronics **9**, 1081 (2020).
5. Y. T. Wan, S. Zhang, J. C. Norman, M. J. Kennedy, W. He, S. T. Liu, C. Xiang, C. Shang, J. J. He, A. C. Gossard, and J. E. Bowers, "Tunable quantum dot lasers grown directly on silicon," Optica **6**, 1394–1400 (2019).
6. D. Benedikovic, L. Virot, G. Aubin, J. M. Hartmann, F. Amar, X. Le Roux, C. Alonso-Ramos, E. Cassan, D. Marris-Morini, P. Crozat, F. Boeuf, J. M. Fedeli, C. Kopp, B. Szelag, and L. Vivien, "40 Gbps heterostructure germanium avalanche photo receiver on a silicon chip," Optica **7**, 775–783 (2020).
7. J. Witzens, "High-speed silicon photonics modulators," Proc. IEEE **106**, 2158–2182 (2018).
8. D. X. Dai, L. Liu, S. M. Gao, D. X. Xu, and S. L. He, "Polarization management for silicon photonic integrated circuits," Laser Photon. Rev. **7**, 303–328 (2013).
9. D. X. Dai and J. E. Bowers, "Silicon-based on-chip multiplexing technologies and devices for peta-bit optical interconnects," Nanophotonics **3**, 283–311 (2014).
10. J. Zhang, T.-Y. Liow, G.-Q. Lo, and D.-L. Kwong, "10Gbps monolithic silicon FTTH transceiver without laser diode for a new PON configuration," Opt. Express **18**, 5135–5141 (2010).
11. L. Xu, Q. Li, N. Ophir, K. Padmaraju, L.-W. Luo, L. Chen, M. Lipson, and K. Bergman, "Colorless optical network unit based on silicon photonic components for WDM PON," IEEE Photon. Technol. Lett. **24**, 1372–1374 (2012).
12. S. Straullu, P. Savio, G. Franco, R. Gaudino, V. Ferrero, S. Bernabe, M. Fournier, V. Muffato, S. Menezo, B. Charbonnier, E. Temporiti, D. Baldi, G. Minoia, M. Repossi, L. Carroll, J. Lee, P. O'Brien, R. Marchetti, G.-H. Duan, F. Saliou, and S. Abrate, "Demonstration of a partially integrated silicon photonics ONU in a self-coherent reflective FDMA PON," J. Lightwave Technol. **35**, 1307–1312 (2017).
13. Y. C. Shi, J. Y. Chen, and H. N. Xu, "Silicon-based on-chip diplexing/triplexing technologies and devices," Sci. China Inform. Sci. **61**, 080402 (2018).
14. J. Y. Chen, L. Liu, and Y. C. Shi, "A polarization-insensitive dual-wavelength multiplexer based on bent directional couplers," IEEE Photon. Technol. Lett. **29**, 1975–1978 (2017).
15. H. H. Chang, Y. H. Kuo, R. Jones, A. Barkai, and J. E. Bowers, "Integrated hybrid silicon triplexer," Opt. Express **18**, 23891–23899 (2010).
16. "Gigabit-capable passive optical networks (G-PON): enhancement band," ITU-T Recommendation G.984.5 (2018), https://www.itu.int/rec/T-REC-G.984.5/en.
17. S. H. Jeong, Y. Onawa, D. Shimura, H. Okayama, T. Aoki, H. Yaegashi, T. Horikawa, and T. Nakamura, "Polarization diversified 16λ demultiplexer based on silicon wire delayed interferometers and arrayed waveguide gratings," J. Lightwave Technol. **38**, 2680–2687 (2020).
18. X. F. Lin, T. T. Lang, and J.-J. He, "Design analysis and experimental verification of cross-order AWG triplexer based on silica-on-silicon," J. Lightwave Technol. **29**, 1407–1413 (2011).
19. S. Pathak, P. Dumon, D. Van Thourhout, and W. Bogaerts, "Comparison of AWGs and echelle gratings for wavelength division multiplexing on silicon-on-insulator," IEEE Photon. J. **6**, 4900109 (2014).
20. Y. Tan and D. X. Dai, "Silicon microring resonators," J. Opt. **20**, 054004 (2018).
21. H. N. Xu, L. Liu, and Y. C. Shi, "Polarization-insensitive four-channel coarse wavelength-division (de)multiplexer based on Mach-Zehnder interferometers with bent directional couplers and polarization rotators," Opt. Lett. **43**, 1483–1486 (2018).
22. D. J. Liu, H. N. Xu, Y. Tan, Y. C. Shi, and D. X. Dai, "Silicon photonic filters," Microw. Opt. Technol. Lett., 1–17 (2020).
23. D. J. Liu, M. Zhang, Y. C. Shi, and D. X. Dai, "Four-channel CWDM (de)multiplexers using cascaded multimode waveguide gratings," IEEE Photon. Technol. Lett. **32**, 192–195 (2020).
24. D. J. Liu, M. Zhang, and D. X. Dai, "Low-loss and low-crosstalk silicon triplexer based on cascaded multimode waveguide gratings," Opt. Lett. **44**, 1304–1307 (2019).
25. D. X. Dai, C. L. Li, S. P. Wang, H. Wu, Y. C. Shi, Z. H. Wu, S. M. Gao, T. G. Dai, H. Yu, and H. K. Tsang, "10-channel mode (de)multiplexer with dual polarizations," Laser Photon. Rev. **12**, 1700109 (2018).
26. D. X. Dai and H. Wu, "Realization of a compact polarization splitter-rotator on silicon," Opt. Lett. **41**, 2346–2349 (2016).